FEC2018

Neutron flux distributions in the LHD torus hall evaluated by an imaging plate technique in the first campaign of deuterium plasma experiment

Makoto Kobayashi[1,2], Tomoyo Tanaka[3], Takeo Nishitani[1], Kunihiro Ogawa[1,2], Mitsutaka Isobe[1,2], Gen Motojima[1,2], Akemi Kato[1], Sachiko Yoshihashi[3], Masaki Osakabe[1,2], and LHD experiment group

[1]National Institute for Fusion Science, National Institutes of Natural Sciences, Toki, Japan.
[2]SOKENDAI (The Graduate University for Advanced Studies), Toki, Japan.
[3]Nagoya University, Nagoya, Japan.
E-mail: kobayashi.makoto@nifs.ac.jp

Abstract
The global flux distributions for thermal, epi-thermal and fast neutrons in the torus hall of large fusion devices were experimentally evaluated for the first time in the Large Helical Device (LHD) using the activation foil method measured by the imaging plate (IP) and High-purity Germanium detector (HPGe). It turned out that the thermal neutron was effectively absorbed by borated polyethylene blocks placed beneath the LHD. This should reduce the radioactivity of the floor and is beneficial to maintain good environment for radiation workers. The uniform distributions of epi-thermal neutron and fast neutrons were observed near LHD. In particular, the significant decrease of fast neutron flux with increasing the distance from LHD due to quick energy loss of fast neutron was observed. The neutron flux distribution measurement with rough energy discrimination based on the threshold energy of neutron activation foil allows us to estimate the spatial radiation dose rate as well as the radioactivity in components in the torus hall. The prediction of the radioactivity in the concrete floor indicated that radioactive isotope, ^{55}Fe will be a dominant source of radioactivity in the concrete after nine-years deuterium experiment campaign finished.

1. Introduction

The experiments with deuterium plasma (deuterium plasma experiment) began in March 2017 in the Large Helical Device (LHD), which is one of the largest superconducting fusion plasma experimental machines in the world. The deuterium fusion reaction produces neutrons and tritium. Therefore, an appropriate radiation control for safe operation is of importance. The National Institute for Fusion Science (NIFS) has established the institutional radiation control regulations for deuterium plasma experiment [1,2]. This regulation limits the release of radiation into the environment in order to obtain public acceptance for the deuterium plasma experiment in LHD.

For the safe operation of deuterium plasma in LHD, the radiation control inside the torus hall is important, as well. Neutron will be captured by many components in the torus hall, then, makes them radioactive. The activated materials emit gamma/beta rays which cause a radiation dose for workers. Also, the radiation field in the torus hall occasionally produces malfunctions in highly integrated electric components such as programmable logic controller (PLC) [3,4]. Therefore, the estimation of the radiation field produced by neutron transport is important for steady operation of LHD.

The other important purpose of radiation control is to plan the decommissioning of LHD in future. In the decommissioning of LHD, the radioactivity of components such as LHD body, heating system, diagnostics, and concrete walls should be evaluated precisely. The neutron distribution in the torus hall, which allows us to predict the radioactivity in the torus hall proceeding with the deuterium plasma experiment in LHD, is required. The prediction of neutron transport and consequent radioactivity in materials during deuterium experiment in LHD has been estimated by using DORT 3.5, which is a two-dimensional neutron transport code, combined with CINAC code [5]. In addition, the three-dimensional neutron transport model using a General Monte Carlo N-Particle Transport (MCNP) code was developed for LHD [6]. However, in both cases, many components around LHD were absent in the calculation, although the neutron transport calculation relies on the precise input geometry data. As is the case with LHD, the fusion devices including ITER, DEMO, commercial reactors, and their torus halls will have a large size with many components. As the complex components of fusion devices and the characteristics of neutron by which neutron can stream through a narrow pass, it is necessary to acquire the neutron flux distribution in the torus hall by actual measurements. This paper reviews the experimental evaluation of the global flux distributions for fast, epi-thermal and thermal neutrons in the torus hall measured in the first campaign of the deuterium plasma experiment in LHD. The activation foil method using indium (In), gold (Au) and nickel (Ni) was applied for neutron flux measurement. Although the activation

foil method is a typical method to measure neutron flux even in the field of fusion research [7,8], this work is a first precise evaluation of neutron flux distribution discriminating the neutron energy utilizing several tens of various activation foils placed in the torus hall of a large fusion device, which will be a benchmark not only for LHD but also for other devices such as ITER and DEMO. The radioactivity of the foils was evaluated by the High-purity Germanium detector (HPGe) for precise radioactivity determination and the imaging plate (IP) method for measuring the plenty of samples in a short time. In addition, according to the neutron flux distribution obtained in this work, the radioactivity in the plain concrete, which is the dominant component as floors and walls of the LHD torus hall, during/after the deuterium experiment in LHD were evaluated.

2. The component layout in the LHD torus hall

The torus hall of LHD has the size of W75, L45, and H40 m^3. The walls of the torus hall are made of plain concrete. The thicknesses of the walls and the floor of the torus hall are 2 m. The details of the component layout in the torus hall are shown in Fig. 1. The vacuum vessel of LHD is equipped with two helical coils and six poloidal field coils. These coils are covered by the cryostat to prevent the air exposure to the surface of coils for cooling. The plasma of deuterium is generated by heating deuterium. Then, the neutron generates by the fusion reaction.

The components for heating plasma, diagnostics of plasma, and other purposes are connected to LHD [9,10]. A major heating system in LHD is Neutron Beam Injector (NBI) [11]. There are five NBIs for LHD. Three of them can inject neutral beam into the plasma tangentially, and are called as t-NBI (#1, #2, #3). The two others perpendicularly inject the neutral beam, and are described as p-NBI (#4, #5) in Fig. 1. In NBI, a part of the energetics deuterium collide with deuterium retained in the beam dump. Therefore, neutron will be generated. In the present study, several combinations of hydrogen and deuterium were used as the source gas in NBI. However, the neutron flux distribution in the torus hall should be independent on the source gas of each NBI because the neutron yield in the beam bump of NBI is estimated to be 3 orders of magnitude lower than that by the LHD plasma [1].

Neutron yield during deuterium plasma experiments were measured by the neutron flux monitors (NFM), which are located at the top of LHD center axis (#1), near the large outside port on the mid plane (#2, #3), consisting of ^{235}U fission chamber, ^{10}B counter,

and ^{3}He counter [12-14]. The neutron activation system (NAS) is also equipped in LHD, which consists of pneumatic tubes to send the activation foils near the vacuum vessel, for the cross-check of NFM. The details of NAS is available in Ref. [15].

The borated polyethylene blocks were used as the neutron shield for components. Polyethylene effectively decelerate the kinetic energy of neutron generated in the deuterium plasma. Then, boron contained in the polyethylene blocks captures thermal neutron by the large cross-section of ^{10}B(n,α)^{7}Li reaction [17]. The borated polyethylene blocks contain 10 % boron. On the floor underneath LHD, the borated polyethylene blocks were placed like a disc with the inner radius of ~ 2.3 m, outer radius of ~ 6.9 m, and the thickness of 5 cm. Exceptionally, un-borated polyethylene blocks were used just below the 8.5-L port of LHD, which is the west side of LHD as seen in Fig. 1, and they occupied 36 degrees of disc-shaped polyethylene blocks underneath LHD.

3. Experimental

3.1 Activation foil

As the activation foil, In, Au and Ni were selected in this work. The radioactive isotopes of these activation foils emit gamma-ray with specific energy. In and Au has the large cress-section to capture thermal neutron. In has two isotopes as ^{113}In and ^{115}In. The natural abundances of these indium isotopes are 4.3 % and 95.7 %, respectively. Thermal neutrons react with ^{115}In as ^{115}In(n,γ)^{116m}In. The minor isotope of indium as ^{113}In also reacts with thermal neutron as ^{113}In(n, γ)^{114m}In. The half-lives of ^{114m}In and ^{116m}In are 49.5 days and 54.3 minutes, respectively [18]. Au exists in nature as ^{197}Au (100 % abundance). Neutrons react with ^{197}Au as ^{197}Au(n,γ)^{198}Au. The half-life of ^{198}Au is 2.7 days [18]. In this study, Au foils were covered by cadmium (Cd) filters with the thickness of 1 mm. Cd has the capability for absorbing thermal neutrons. Epi-thermal neutron can penetrate Cd filter to react with Au foil. It was assumed in this study that the radioactivity in the Au foil with Cd filters are only caused by epi-thermal neutron. ^{58}Ni is a major isotope of nickel (About 68 % of natural abundance). The reaction of ^{58}Ni(n,p)^{58}Co has a threshold energy to occur. Therefore, fast neutron can produce ^{58}Co in Ni. The half-life of ^{58}Co is 70.8 days. Therefore, Ni foils were used as a fast-neutron detector in this study. In and Au foils were cut into 0.5 × 0.5 mm^{2}. The thickness of In foils was 0.5 mm, and that of Au foils was 0.1 mm. The size of Ni foils was 20 × 20 × 2 mm^{3} to increase the radioactivity.

Finally, these foils were put into plastic bags for neutron irradiation.

3.2 Neutron irradiation in the torus hall

In the weekly operation of LHD, the first weekday is assigned for maintenance work. The other weekdays are for experiment. The samples were placed on the floor of the LHD torus hall on the maintenance day. The positions where In, Au, and Ni foils are presented in Fig. 4, Fig. 5, and Fig. 6 with the red colored circles, respectively. In foils were irradiated with neutron in the LHD torus hall for one day. Au foils with Cd filter were irradiated with neutrons for one week. Ni foils were exposed to neutron in the torus hall for two months in order to accumulate the radioactivity. However, the fast-neutron measurement by Ni foils placed far away from LHD was not tried in this campaign because the radioactivity in Ni foils will be below the detection limit (~10^{-2} Bq/g) of HPGe in that region. After certain neutron irradiation duration, the samples were taken out from the torus hall for analysis. In particular, for In, because of the fast decay rate of ^{116m}In, all foils were salvaged from the torus hall within several hours after daily experiment finished. For Au, foils were taken out from the torus hall after 2 days passed from the last plasma operation.

3.3 Evaluation of the neutron flux distribution

One of the analysis systems used in this work was HPGe. HPGe has the capability to identify the radioactive isotopes by gamma-ray energy spectrometry. HPGe also can evaluate the precise quantity of radioactive isotopes. However, this method requires a longer time to measure one sample. The HPGe detector used in this work was of Canberra Industries, Inc. (Model: GX3018/CP5-PLUS-U). Because the detector is in a lead shield with the thickness of 100 mm, the influence of external background radiation is sufficiently reduced. Output pulses from preamplifier are fed into multichannel analyzer, DSA-LX of Canberra.

The other method was IP. IP is a sheet type detector which can store the energy transferred from radiation [19]. IP can release the integrated stored-energy as photo-stimulated luminescence (PSL) by laser injection. IP is usually applied for two-dimensional visualization of the radiation source as it has the capability to measure a large surface area.

The IP sheet used in this work was BAS-SR 2040 manufactured by FUJIFILM.

Samples after salvaging were mounted on the mylar file with the thickness of 100 μm as shown in Fig. 2. The PSL values were measured by image reader as Typhoon FLA 9500 of GE Healthcare. The average PSL values over the foil surface area were calculated by using a software of Image Quant TL developed by GE Healthcare. The background PSL value was subtracted by measuring the PSL values for the region away from foils. In this work, the calibration of the PSL value to convert the radioactivity in the foils were carried out by measuring several foils by HPGe. The conversion factors from the PSL to radioactivity were obtained. The details of these analyses were described in our previous work [20]. For Ni, due to the low radioactivity in the foil and enough longer half-life, all samples were measured by HPGe.

The radioactivity in the foil measured by HPGe and IP correlates with the neutron fluence. The neutron flux at the position of the foil was evaluated by the following equation,

$$\frac{dN^{(A)}}{dt} = N^{(S)}\sigma\phi - \frac{\ln 2}{T_{1/2}} N^{(A)} \quad (1).$$

Here, $N^{(A)}$ and $N^{(S)}$ are the amounts of radioactive and stable isotopes, respectively, and ϕ presents the neutron flux [cm^{-2} s^{-1}] and $T_{1/2}$ is the half-life [s]. The reaction cross-section, σ [cm^2], is dependent on the neutron energy. The value of σ is different for each activation foil and place where activation foils were set. In this study, σ was evaluated by MCNP6 calculation based on our previous work [2156.

]. The $N^{(A)}$ is zero before the neutron irradiation. Note that neutron flux is different in each deuterium plasma operation, and $N^{(A)}$ is determined by the integration of these different neutron fields. On the other hand, the source and the energy of neutron are almost the same in every deuterium plasma operation. Therefore, only ϕ is different in every plasma, and ϕ is proportional to neutron yield which was measured by NFM.

4. Prediction of radioactivity in concrete floor proceeding with deuterium experiment

The prediction of radioactivity in the concrete floor proceeding with deuterium

experiment was evaluated by using the neutron flux distribution estimated in this work. The DCHAIN-SP code bundled in PHITS code was used for activation calculation [22]. DCHAIN-SP requires the composition of concrete, the irradiation time, cooling time, the neutron energy spectrum and the neutron flux to estimate the radioactivity.

The composition of plain concrete adopted in this study is as same as that used in our previous study [5]. The weight percent of hydrogen, oxygen, silicon, aluminum, calcium, sulfur, iron, magnesium, sodium, and potassium are 0.54, 47.98, 30.41, 4.40, 7.95, 0.12, 4.88, 0.23, 1.64, and 1.85, respectively. Note that the minor elements in concrete such as cesium, cobalt and europium were not considered in this study [23].

For the irradiation time and cooling time, the plasma operation period for four months and the maintenance period for eight months were assumed as an annual operation according to the previous experimental campaigns. The deuterium experiment in LHD is planned for nine years. The maximum of annual neutron yield in the first six years are 2.1×10^{19}, and the last three years are 3.2×10^{19}.

The neutron flux and neutron energy spectrum were tentatively evaluated by MCNP6 code and corrected by the results of actual neutron flux measurement by activation foils in this study. The model for MCNP6 calculation used in this work includes LHD body, the cryostat, the torus hall, and the basement of the torus hall. Pipes and ducts between the torus hall and the basement were also taken into account. The polyethylene blocks underneath LHD were also considered. This model for MCNP6 calculation has been already applied for the calibration of NFM in LHD, and the details of this model can be found in Ref. [20]. With this model, the nuclear data library of ENDF/B-VII.1 was used [24]. The calculation was performed until the statistical error became less than 0.1.

In this study, the neutron was separated by its kinetic energy into the thermal neutron, epi-thermal neutron, and fast neutron which are defined as the neutron with the energy ranged below 0.55 eV, 0.55 eV-100 keV, and above 100 keV, respectively. The fluxes for thermal neutron, epi-thermal neutron and fast neutron estimated by MCNP6 calculation were corrected by the neutron flux evaluated by In foils, Au foils with Cd filter, and Ni foils, respectively.

5. Results and discussion

5.1 Neutron flux distribution

The typical gamma-ray spectra obtained by HPGe measurements for In, Au, Ni are shown in Fig. 3. For In, there were many peaks at 417, 819, 1097, and 1294 keV, which are caused by ^{116m}In. For Au, a major gamma-ray peak at 411 keV was observed. This peak was attributed to gamma-ray by ^{198}Au. In the measurement for Ni foils, there were two major peaks. One of them was located at 811 keV, and this gamma-ray was emitted by ^{58}Co. The other peak at 511 keV should be generated by the electron-positron annihilation. Because ^{58}Co decays with electron capture and β^+ decay mode, the positron emitted in β^+ decay process reacted with electron in the HPGe system and was detected. The peak areas in these spectra corresponded to the radioactive isotopes in foils.

The thermal neutron distribution on the floor level of the LHD torus hall measured by In foils is shown in Fig. 4 [16]. In this figure, the thermal neutron flux, ε_{th}, is defined as the local thermal neutron flux for single neutron source. The mapping of flux distribution was done by using GMT (Generic Mapping Tool), ver. 5. The thermal neutron flux distribution was concentrated within about 15 m from the center of LHD. The relatively high thermal neutron flux was observed at the position underneath the 8.5-L port and the center of LHD. As described in Section 2, polyethylene blocks were placed like a disc shape underneath LHD. Most of the blocks contain 10 % of boron to absorb thermal neutron. However, the polyethylene blocks were absent in the center part of LHD. Fast neutrons from LHD were thermalized effectively in the concrete floor as it contains a large amount of water, resulting in the relatively high thermal neutron flux there. Besides, the un-borated polyethylene blocks were placed underneath the 8.5L port of LHD. Because of the absence of thermal neutron absorber in the polyethylene blocks, the fast neutrons were effectively converted to thermal neutrons there. Consequently, the borated polyethylene blocks effectively worked to reduce the radioactivity underneath LHD.

Fig. 5 shows the flux distribution of epi-thermal neutron in the torus hall experimentally evaluated by the Au foils with Cd thermal neutron absorber [25]. Unlike thermal neutron distribution shown in Fig. 4, the epi-thermal neutron distribution showed almost uniform flux underneath LHD. The epi-thermal neutrons were generated by the deceleration processes of fast neutron. As is the case with thermal neutron, polyethylene blocks would effectively convert fast neutrons to epithermal neutrons. However, boron inside the polyethylene blocks would not largely capture epi-thermal neutron because the cross section of ^{10}B(n,α)^{7}Li reaction is almost proportional to the reciprocal of the square root of the neutron kinetic energy [16]. Consequently, the uniform distribution of epi-thermal

neutron underneath LHD is reasonable.

Fast-neutron flux distribution around LHD is described in Fig. 6. The fast-neutron flux distribution away from LHD was not measured in this study as explained in section 3.2. Therefore, fast-neutron distribution near LHD was evaluated in Fig. 6. The almost uniform distribution of fast neutron underneath LHD was observed. The flux of fast neutron near the LHD was about one order of magnitude higher than that of thermal neutron. The fast-neutron flux was decreased sharply with increasing the distance from LHD increased compared to those of thermal neutron and epi-thermal neutron due to the quick energy loss process of fast neutron with components.

5.2 Activation evaluation for the concrete floor

According to Figs. 4, 5, and 6, the neutron flux should be totally largest underneath 8.5-L port on the floor level. Therefore, the radioactivity in the top-surface of concrete floor at this position is valuable from the safety point of view. The predicted radioactivity in the concrete floor underneath 8.5-L port is shown in Fig. 7. The major radioactive nuclides were ^{40}K, ^{37}Ar, ^{55}Fe, ^{45}Ca, ^{32}P, ^{54}Mn, and ^{39}Ar during deuterium experiment. For the clearance of the radioactivated components, the artificial radioactivity below 0.1 Bq g^{-1} is required. It is well known that ^{40}K is natural radioactive isotope. The radioactivities by ^{37}Ar, ^{45}Ca, ^{32}P, and ^{54}Mn quickly decreased after nine-years deuterium experiment campaign finished due to the relatively short half-lives. Therefore, the radioactivity of ^{55}Fe should be controlled. It was predicted that more than ten years will be required to wait for ^{55}Fe being below 0.1 Bq g^{-1} after the end of deuterium experiment campaign. The major generation channel of ^{55}Fe should be ^{54}Fe(n,γ)^{55}Fe reaction, which mainly occurs by thermal neutron. Therefore, as is the case with other position underneath LHD, the installation of thermal neutron absorber such as borated polyethylene blocks underneath 8.5-L port is available to mitigate the cooling time for ^{55}Fe in the concrete floor.

Also, the minor elements in the concrete such as cesium, cobalt and europium were not considered in this study, although these elements usually create radioactive isotopes with longer half-life [23]. The validity check for the prediction in this study by the actual gamma-ray spectroscopy measurement for concrete will be done in future.

5. Summary

The flux distributions of thermal, epi-thermal and fast neutrons on the floor level of the LHD torus hall in the first campaign of deuterium plasma experiments in LHD were experimentally evaluated by using activation foils and by applying the IP and HPGe measurements. The relatively high thermal neutron fluxes were observed around the 8.5-L port and the center of LHD. The borated polyethylene blocks worked well to reduce thermal neutron flux and subsequent activation of components. Unlike thermal neutron, the fluxes of epi-thermal neutron and fast neutron underneath LHD were almost uniform. Because the ratio of 2.45 MeV and 14.1 MeV neutrons generated in the deuterium plasma in LHD would not largely change, the distribution obtained in this work will be available for the future campaigns of deuterium plasma experiment. According to these results, the prediction of radioactivity in the concrete floor proceeding with deuterium experiments were carried out for the decommissioning of the torus hall. The radioactivity by ^{55}Fe should be a major radioactive isotope in the concrete. The radioactivity below 0.1 Bq g^{-1} will be achieved by elapsing more than eleven years after the nine-years deuterium experiment in LHD finished.

ACKNOWLEDGMENTS

This work was supported by LHD project budget (ULGG801, ULAA027). This work is performed with the support and under the auspices of the NIFS Collaboration Research program (NIFS18KESA030). The authors wish to thank the technical groups for their assistance in this work.

REFERENCES

[1]. OSAKABE M., ISOBE M., TANAKA M., MOTOJIMA G., TSUMORI K., YOKOYAMA M., MORISAKI T., TAKEIRI Y. and LHD EXPERIMENT GROUP, “Preparation and commissioning for the LHD deuterium experiment”, IEEE Transaction on Plasma Science, **46** (2018) 2324-2331.

[2]. SAFETY MANAGEMENT PLAN FOR LHD DEUTERIUM PLASMA EXPERIMENT, (2017) (http://www.nifs.ac.jp/j_plan/pamph_030.pdf , [in Japanese]).

[3]. OGAWA K., NISHITANI T., ISOBE M., MURATA I., HATANO Y., MATSUYAMA S., NAKANISHI H., MUKAI K., SATO M., YOKOTA M., "Investigation of irradiation effects on highly integrated leading edge electronic components of diagnostics and control systems for the LHD deuterium operation", Nuclear Fusion, **57** (2017) 086012.

[4]. OGAWA K., NISHITANI T., ISOBE M., SATO M., YOKOTA M., HAYASHI H., KOBUCHI T., NISHIMURA T., "Effects of gamma-ray irradiation on electronic and non-electronic equipment of Large Helical Device", Plasma Science and Technology, **19** (2017) 025601.

[5]. NISHIMURA K., YAMANISHI H., HAYASHI K., KOMORI A., "Activation analysis for LHD experiments with deuterium gases", Plasma and Fusion Research, 3 (2008) S1024.

[6]. PELOWITS D.B. (Ed.), MCNP6 users Manual, LA-CP-13-00634, Los Alamos National Laboratory, (2013).

[7]. PROKOPOWICZ R., SCHOLZ M., SZYDLOWSKI A., POPOVICHEV S., "Measurements of neutron yield from deuterium plasmas at JET by activation techniques", AIP Conference Proceedings, **993** (2008) 251.

[8]. BERTALOT L., ROQUEMORE A.L., LOUGHLIN M., ESPOSITO B., "Calibration of the JET neutron activation system for DT operation", Review of Scientific Instruments **70** (1999) 1137.

[9]. TAKEIRI Y., "The Large Helical Device: entering deuterium experiment phase toward steady-state helical fusion reactor based on achievements in hydrogen experiment phase", IEEE Transaction on Plasma Science, **46** (2018) 2348-2353.

[10]. KOMORI A., YAMADA H., IMAGAWA S., KANEKO O., KAWAHATA K., MUTOH K., OHYABU N., TAKEIRI Y., IDA K., MITO T., NAGAYAMA Y., SAKAKIBARA S., SAKAMOTO R., SHIMOZUMA T., WATANABE K.Y., MOTOJIMA O., LHD EXPERIMENT GROUP, "Goal and achievements of Large Helical Device project", Fusion Science and Technology, **58** (2010) 1-11.

[11]. TAKEIRI Y., KANEKO O., TSUMORI K., OSAKABE M., IKEDA K., NAGAOKA K., NAKANO H., ASANO E., KONDO T., SATO M., SHIBUYA M., KOMADA S., "LHD Experiment Group, High performance of neutral beam injectors for extension of LHD operational regime", Fusion Science and Technology, **58** (2010) 482-488.

[12]. ISOBE M., OGAWA K., MIYAKE H., HAYASHI H., KOBUCHI T., NAKANO Y., WATANABE K., URITANI A., MISAWA T., NISHITANI T., TOMITAKE M., KUMAGAI T., MASHIYAMA Y., ITO D., KONO S.,

YAMAUCHI M., TAKEIRI Y., “Wide dynamic range neutron flux monitor having fast time response for the Large Helical Device”, Rev. Sci. Instrum, **85** (2014) 11E114.

[13]. NISHITANI T., OGAWA K., ISOBE M., “Monte Carlo simulation of the neutron measurement for the Large Helical Device deuterium experiments”, Fusion Eng. Des., **123** (2017) 1020-1024.

[14]. ISOBE M., OGAWA K., NISHITANI T., PU N., KAWASE H., SEKI R., NUGA H., TAKADA E., MURAKAMI S., SUZUKI Y., YOKOYAMA M., OSAKABE M., AND LHD EXPERIMENT GROUP, “Fusion neutron production with deuterium neutral beam injection and enhancement of energetic-particle physics study in the large helical device”, Nuclear Fusion **58** (2018) 082004.

[15]. PU N., NISHITANI T, ISOBE M., OGAWA K., KAWASE K., TANAKA T., LI S.Y., YOSHIHASHI S., URITANI A, In situ calibration of neutron activation system on the large helical device, Re. Sci. Instrum., **88** (2017) 113302.

[16]. SHIBATA K., IWAMOTO O., NAKAGAWA T., IWAMOTO N., ICHIHARA A., KUNIEDA S., CHIBA S., FURUTAKA K., OTUKA N., OHSAWA T., MURATA T., MATSUNOBU H., ZUKERAN A., KAMADA S., AND KATAKURA J., JENDL-4.0: A New Library for Nuclear Science and Engineering, Journal of Nuclear Science and Technology **48** (2011) 1-30.

[17]. KOBAYASHI M., TANAKA T., NISHITANI T., OGAWA K., ISOBE M., KATO K., SAZE T., YOSHIHASHI S., OSAKABE M., LHD EXPERIMENT GROUP, “First measurements of thermal neutron flux distribution in LHD torus hall generated by deuterium plasma experiments”, Fusion Engineering and Design, **137** (2018) 191-195.

[18]. FIRESTONE R. B., Table of isotopes 8th edition, John Wiley & Sons, Inc. 1996.

[19]. GONZALEZ A. L., MITCH H. LI, M., TOLK N., DUGGAN D. M., “Energy response of an imaging plate exposed to standard beta sources”, Applied Radiation and Isotopes, **57** (2002) 875-882.

[20]. KOBAYASHI M., NISHITANI T., KATO A., SAZE T., TANAKA T., YOSHIHASHI S., OGAWA K., ISOBE M., “Evaluation of imaging plate measurement for activated indium as fast-neutron detector in large radiation field”, Progress of Nuclear Science and Technology, **6** (2019) 58-62.

[21]. NISHITANI T., OGAWA K., KAWASE H., PU N., OZAKI T., ISOBE M., “Monte carlo calculation of the neutron and gamma-ray distributions inside the LHD experimental building and shielding design for diagnostics”, Progress in Nuclear Science and Technology, **6** (2019) 48-51.

[22]. SATO T., IWAMOTO Y., HASHIMOTO S., OGAWA T., FURUTA T., ABE S., KAI T., TSAI P., MATSUDA N., IWASE H., SHIGYO N., SIHVER L., NIITA K., "Features of particle and heavy ion transport code system (PHITS) version 3.02", Journal of Nuclear Science and Technology, **55** (2018) 684-690.

[23]. SUZUKI A., IIDA T., MORIIZUMI J., SAKUMA Y., TAKADA J., YAMASAKI K., YOSHIMOTO T., "Trace elements with large activation cross section in concrete materials in Japan", Journal of Nuclear Science and Technology, **38** (2001) 542-550.

[24]. CHADWICK M.B., HERMAN M., OBLOŽINSKÝ P., DUNN M.E., DANON Y., KAHLER A.C., SMITH D.L., PRITYCHENKO B., ARBANAS G., ARCILLA R., BREWER R., BROWN D.A., CAPOTE R., CARLSON A.D., CHO Y.S., DERRIEN H., GUBER K., HALE G.M., YOUNG P.G., ENDF/B-VII.1 Nuclear Data for Science and Technology: Cross Sections, Covariances, Fission Product Yields and Decay Data, Nuclear Data Sheets **112** (2011) 2887-2996.

[25]. TANAKA T., KOBAYASHI M., YOSHIHASHI S., URITANI A., WATANABE K., YAMAZAKI A., NISHITANI T., OGAWA K., ISOBE M., "Measurement of thermal and epithermal neutron flux distribution in the torus hall of LHD using activation method in 1st deuterium experiment campaign", presented in 27th International Toki Conference on Plasma Fusion Research, P2-49, Toki city, Japan Nov. 19-22, 2018.

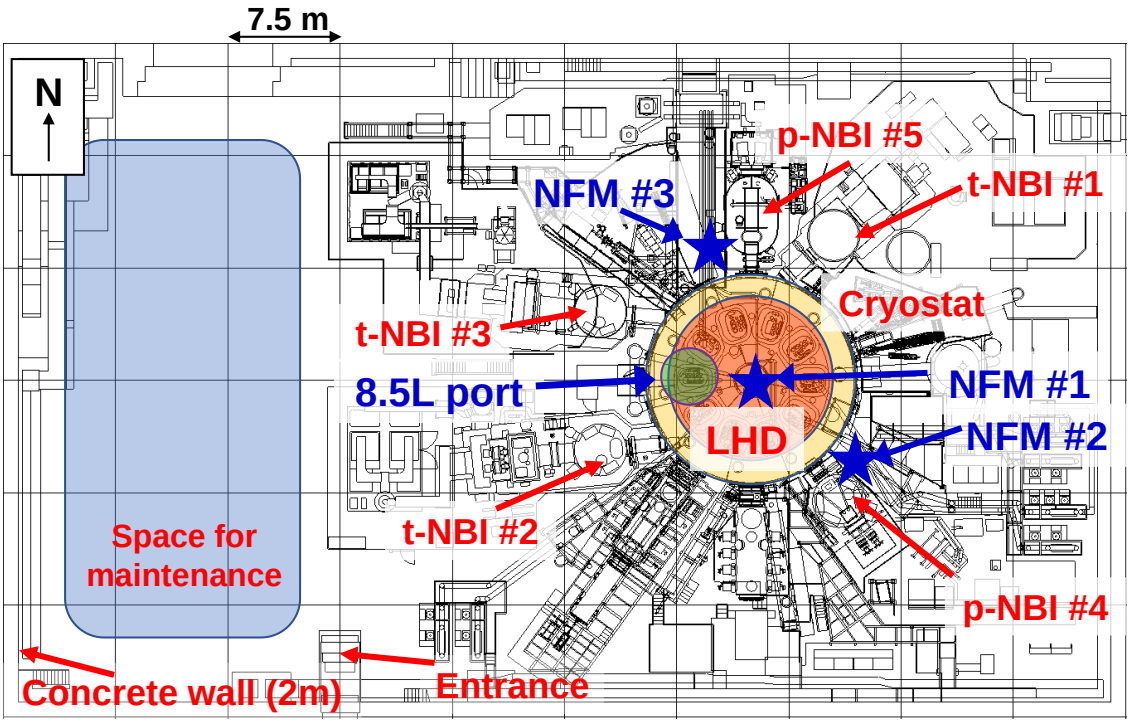

Fig. 1 Component layout of the LHD torus hall [17]

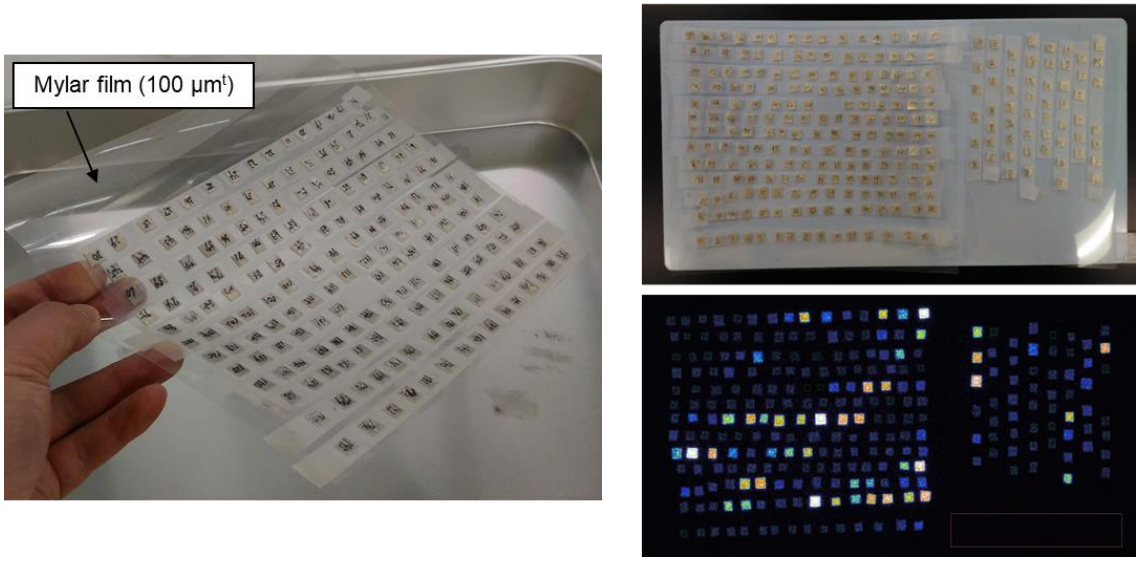

Fig. 2 Foils stuck on the mylar film for IP measurement, and the typical experimental result of IP measurement for In foils.

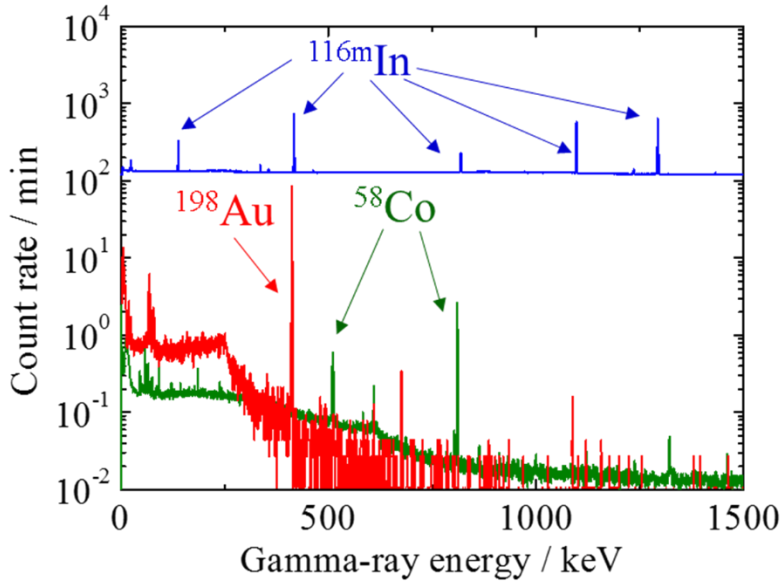

Fig. 3 Typical gamma-ray spectra for In, Au, and Ni foils exposed to neutron in the LHD torus hall.

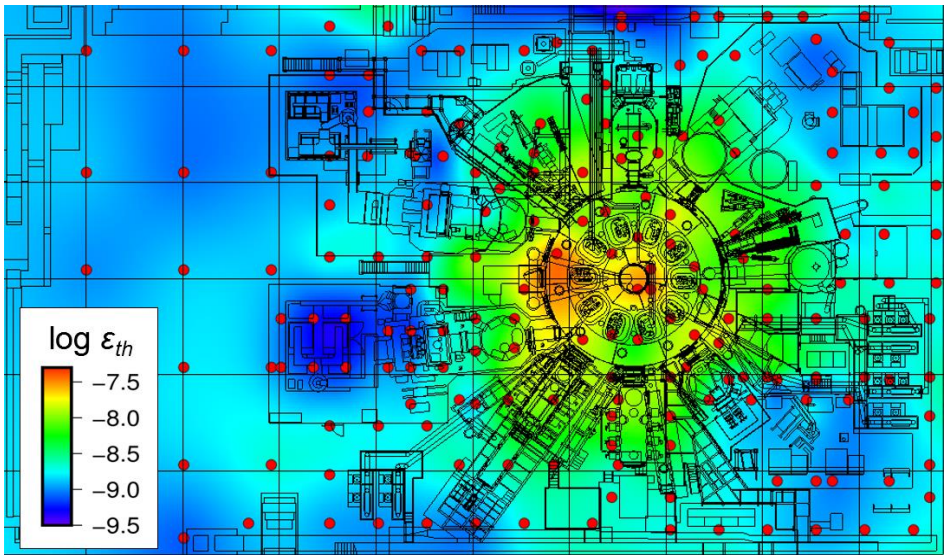

Fig. 4 The thermal neutron flux distributions on the floor level of the LHD torus hall measured by In foils overlaid with two dimensional CAD model of the torus hall [17]. The red circles in this figure express the position of In foils.

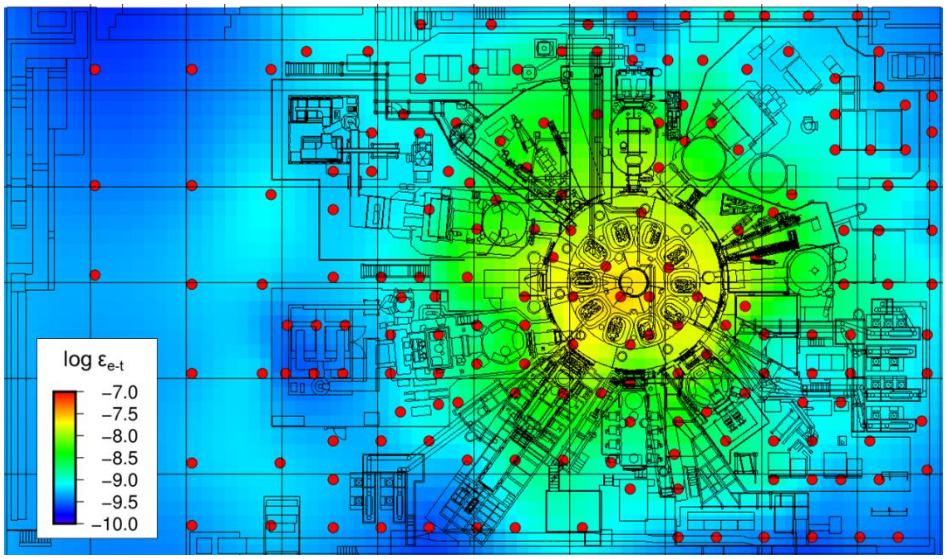

Fig. 5 The epi-thermal neutron flux distributions on the floor level of the LHD torus hall measured by Au foils covered with Cd filter overlaid with two dimensional CAD model of the torus hall [25]. The red circles in this figure express the position of Au foils.

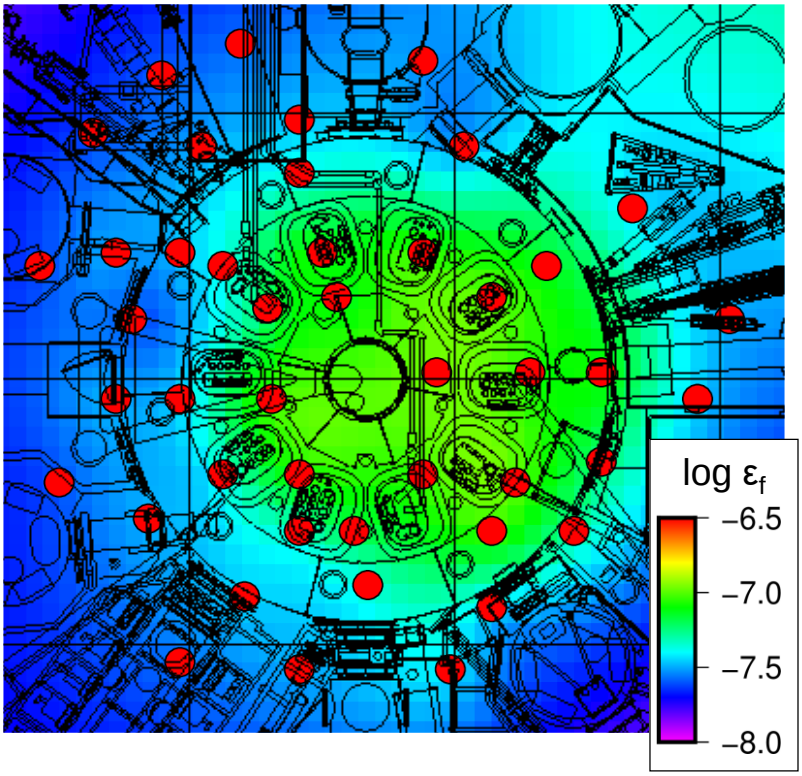

Fig. 6 The fast neutron flux distributions on the floor level near LHD measured by Ni foils, overlaid with two-dimensional CAD model of the torus hall. The red circles express the position of Ni foils.

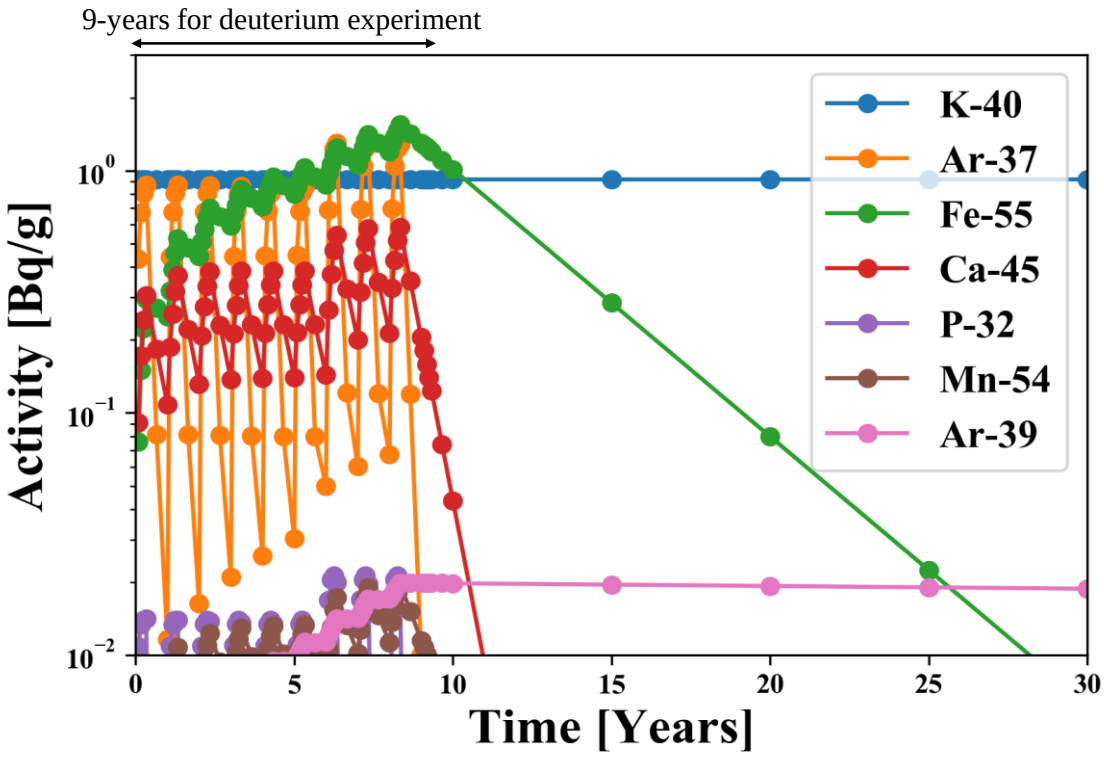

Fig. 7 The radioactivity in the top-surface of concrete floor underneath 8.5-L port proceeding with the deuterium experiment and after the 9-years deuterium experiment campaign.